J. Chem. Sci. Vol. 124, No. 4, July 2012, pp. 763–771.

Does polar interaction influence medium viscosity? A computer simulation investigation using model liquids

SNEHASIS DASCHAKRABORTY and RANJIT BISWAS*

Department of Chemical, Biological and Macromolecular Sciences, S. N. Bose National Centre for Basic Sciences, JD Block, Sector III, Salt Lake, Kolkata 700 098, India
e-mail: ranjit@bose.res.in

MS received 8 October 2011; revised 29 December 2011; accepted 3 January 2012

Abstract. Molecular dynamics simulations of model liquids interacting via Lennard–Jones (L–J) and Stockmayer (SM) interactions have been carried out to explore the effects of the longer-ranged dipole–dipole interaction on solvent viscosity and diffusion. Switching on of the dipolar interaction at a fixed density and temperature has been found to increase the viscosity over that of the LJ liquid, the extent of increase being a few percent to as large as ∼60% depending on the magnitude of the solvent dipole moment used in the SM potential. The simulated translational and rotational diffusion coefficients show strong dipole moment and temperature dependences, eventhough effects of these parameters on solvent–solvent radial distribution function are moderate. Interestingly, a partial solute–solvent decoupling is observed when the simulated translational and rotational diffusion coefficients are connected to the simulated viscosity coefficients via the Stokes–Einstein (SE) and Stokes–Einstein–Debye (SED) relations. In the limit of large dipole moment, simulated self-part of the van Hove correlation function at intermediate times reveals a departure from the Gaussian distribution with particle displacement. This suggests that dynamic heterogeneity is one of the reasons for the departure of centre-of-mass diffusion from the SE relation in these model systems.

Keywords. Stockmayer fluids; dipolar interaction; viscosity; diffusion coefficients; decoupling.

1. Introduction

Viscosity coefficient (η, hereafter simply viscosity) is one of the most important dynamical properties of a fluid as it can be experimentally accessed. In conjunction with diffusion coefficients, translational (D_T) and rotational (D_R), η provides crucial information about solute–solvent coupling.[1,2] Moreover, a molecular level understanding can be achieved via using the macro–micro relationships, for example, that between the experimentally measurable viscosity and the corresponding computationally accessible stress tensor autocorrelation function.[1] This provides a description in which one can modify various molecular properties such as molecular diameter and dipole moment and investigate the subsequent effects on individual transport properties (η and D_x, x being T or R) and also on coupling between them. Thermodynamic parameters like solvent density and temperature can affect at the molecular level the coupling between D_x and η. Traditionally, the coupling is expressed via the hydrodynamic relations, Stokes–Einstein (SE)[1] for the centre-of-mass (translational) motion and Stokes–Einstein–Debye (SED)[2] for the rotational motion. Deviations from SE and SED relations often attract special attention because of the possibility of accessing rich, often new, information regarding dynamical pathways to the environmental coupling.[3–9]

Since the viscosity being discussed here is the shear viscosity and related to the rate of momentum transfer from one fluid layer to the adjacent one while moving,[1] it is expected that the interactions with nearest neighbours would dominate the process. At typical liquid densities, the short range repulsive interactions mainly dictate the spatial distribution of nearest neighbours. Consequently, it has been argued that consideration of only the region around the peak of the static structure factor in calculations would suffice to predict the liquid viscosity.[10,11] One would then be naturally interested to ask the following questions: at typical liquid densities what would be the effects of the longer-ranged dipole–dipole interaction on η and how temperature would modulate such effects? The main focus of this paper is to investigate the above two questions via simulation studies of model liquids. In addition, solute–solvent coupling as a function of the strength of the dipolar interaction (through the variation of molecular dipole

*For correspondence

moment, μ) and temperature have been systematically explored.

We would like to mention here that simulation studies have already explored dependences of viscosity on thermodynamic parameters (temperature, density and pressure) in various model liquids, ranging from L–J neat fluids[12] and binary mixtures[13] to explosive materials.[14] In addition, attempts to correlate viscosity with various physical parameters of a substance have shown viscosity to be proportional to the square root of molar mass, cube root of refractive index and linear to the dipole-moment.[15] These correlations, however, lack microscopic explanations and thus warrant molecular level investigation. Here we have carried out such a study with two different model liquids, namely, Lennard–Jones[1] and Stockmayer (SM) fluids.[16,17] The advantage of choosing such a pair is that SM potential, being a sum-total of L–J and dipole–dipole interactions, facilitates an easy exploration of the effects of dipolar interaction on liquid transport properties by simply changing the magnitude of the molecular dipole moment. Note that applicability of integral equations method has already been tested[18] for predicting the pressure and viscosity of SM fluids. In addition, simulation studies have investigated static dielectric properties,[19–21] dynamic solvation response,[22–25] structural aspects,[26] freezing transition[27] for the neat SM fluids, and interfacial properties of electrolyte solutions[28] and binary mixtures of these model fluids.[29] Therefore, SM fluids are one of the most studied model fluid systems and further studies on the transport properties will help better characterizing these systems.

The rest of the paper is arranged as following. Necessary theoretical discussions and simulation details are presented in the next section. Simulated results and their implications are illustrated in section 3. Concluding remarks are provided in section 4.

2. Simulation details and necessary statistical mechanical relations

Molecular dynamics simulations were performed for one Lennard–Jones system and six Stockmayer (SM) systems covering the dipole moment range from 0.6 to 3.0 Debye in NVT ensembles with a total number of 216 particles in each of the cases at 300 K, 350 K and 400 K (using argon parameters). The non-dipolar system is characterized by the L–J pair potential,

$$V_{LJ}\left(r_{ij}\right) = 4\varepsilon\left[\left(\frac{\sigma}{r_{ij}}\right)^{12} - \left(\frac{\sigma}{r_{ij}}\right)^{6}\right], \qquad (1)$$

where, σ corresponds to the diameter of an L–J particle, r_{ij} the distance between the ith and jth L–J particles, and ε the energy parameter connected to the well-depth. Here, we considered all the systems having particles of same σ and ε which are those of argon, i.e., $\sigma = 3.41$ Å and $\varepsilon/k_B = 119.8$ K, k_B being the Boltzmann constant. The Stockmayer fluids are characterized by the following pair interaction

$$V_{SM}\left(r_{ij}\right) = 4\varepsilon\left[\left(\frac{\sigma}{r_{ij}}\right)^{12} - \left(\frac{\sigma}{r_{ij}}\right)^{6}\right] + \left[\frac{\vec{\mu}_i \cdot \vec{\mu}_j}{r_{ij}^3} - \frac{3}{r_{ij}^5}\left(\vec{\mu}_i \cdot \vec{r}_{ij}\right)\left(\vec{\mu}_j \cdot \vec{r}_{ij}\right)\right], \qquad (2)$$

where the second term in Eq. 2 represents the dipole–dipole interaction ($V_{DD}(r_{ij})$) between ith and jth dipolar particles whose dipole moments are denoted as μ_i and μ_j. Neat systems were only considered and thus $\mu_i = \mu_j$.

The initial configuration was started from a simple cubic lattice in a cubic box with periodic boundary condition and minimum image convention. The scaled density of the system, $\rho^* = \rho\sigma^3 = 0.7$. The volume of the simple cubic box was determined from the density considered. The longer-ranged dipolar interaction was dealt with the Ewald summation technique.[30] The cut-off radius for the L–J and dipolar interaction potentials was taken as half of the box length. Nose–Hoover thermostat[31–33] was employed to maintain constancy of a fixed temperature. Equations of motions were integrated by using the Verlet leapfrog integration scheme[30] with a time-step of 2 fs. First 300 ps of each of the simulation runs were treated as equilibration period and the latter 700 ps as production run. Translational self-diffusion coefficients (D_T) for the L–J and SM systems were calculated from both the mean squared displacements ($\langle|\Delta\vec{r}(t)|^2\rangle$) and velocity autocorrelation functions (VACF). The MSDs were calculated from the simulated centre-of-mass positional vectors $\left(\vec{r}_i^{\,c}(t)\right)$[34,35]

$$\left\langle|\Delta\vec{r}\,(t)|^2\right\rangle = \frac{1}{N}\left\langle\sum_{i=1}^{N}\left|\vec{r}_i^{\,c}(t) - \vec{r}_i^{\,c}(0)\right|^2\right\rangle, \qquad (3)$$

which produced D_T via the connection

$$D_T = \left[\frac{1}{6t}\left(\langle|\Delta\vec{r}(t)|^2\rangle\right)\right]_{t\to\infty}. \qquad (4)$$

D_T from the VACF were obtained by the following manner[34]

$$D_T = \frac{1}{3}\int_0^\infty dt\,\langle\vec{v}_i(t)\cdot\vec{v}_i(0)\rangle, \qquad (5)$$

where, $\vec{v}_i$ is the centre-of-mass velocity vector associated with the ith particle and averaging was done over both time and number of particles.

Rotational diffusion coefficient (D_R) was obtained from the angular velocity autocorrelation function ($C_\omega(t)$) as follows[1,36]

$$D_R \equiv D_R\,(t \to \infty) = \frac{k_B T}{I} \int_0^t ds \left(1 - \frac{s}{t}\right) C_\omega\,(s)\,, \tag{6}$$

where I denote the moment of inertia and $C_\omega\,(t) = \langle \vec{\omega}\,(0) \cdot \vec{\omega}\,(t) \rangle$.

Shear viscosity coefficient (η) was calculated using the Green–Kubo relation,[1]

$$\eta = \frac{V}{k_B T} \int_0^\infty \left\langle P_{\alpha\beta}\,(t)\; P_{\alpha\beta}\,(0) \right\rangle dt, \tag{7}$$

where, $\alpha, \beta = x, y, z$ and $P_{\alpha\beta}$ denotes the off-diagonal term of the pressure tensor

$$P_{\alpha\beta} = \frac{1}{V}\left(\sum_i \frac{p_{i\alpha} p_{i\beta}}{m_i} + \sum_i \sum_{j>i} r_{ij\alpha} f_{ij\beta}\right). \tag{8}$$

As before, the above correlation functions were also averaged over paricles and time.

The pressure can then be readily obtained from the simulated force, $f_{ij\alpha}$, data by employing the following expression

$$\begin{aligned} P &= \frac{1}{3V} \sum_\alpha \left[\sum_i p_{i\alpha} p_{i\alpha}/m_i + \sum_{\mathrm{i}} \sum_{\mathrm{j>i}} r_{ij\alpha} f_{ij\alpha} \right] \\ &= \frac{1}{3V} \sum_\alpha \left[k_B T + \left\{ \sum_i \sum_{j>i} -r_{ij\alpha} \frac{\partial}{\partial r_{ij\alpha}} \right. \right. \\ &\quad \times \left\{ 4\varepsilon \left[\left(\frac{\sigma}{r_{ij\alpha}}\right)^{12} - \left(\frac{\sigma}{r_{ij\alpha}}\right)^{6} \right] \right. \\ &\quad \left. \left. \left. + \left[\frac{\vec{\mu}_{\mathrm{i}} \cdot \vec{\mu}_{\mathrm{j}}}{r_{ij\alpha}^3} - \frac{3}{r_{ij\alpha}^5} \left(\vec{\mu}_{\mathrm{i}} \cdot \vec{\mathrm{r}}_{\mathrm{ij}}\right) \left(\vec{\mu}_{\mathrm{i}} \cdot \vec{\mathrm{r}}_{\mathrm{ij}}\right) \right] \right\} \right\} \right]. \end{aligned} \tag{9}$$

3. Results and discussions

Effects of longer-ranged dipolar interaction and temperature on spatial distribution of particles are depicted in figure 1, where the radial distribution functions (RDFs), $g(r)$, calculated after varying the dipole moment (μ) values at two different temperatures, are shown as a function of the scaled distance ($r^* = r/\sigma$). Note that eventhough the first peak of the RDF increases both with the increase in dipole moment and lowering of temperature, the enhancement factor always remains very small. This indicates that η will increase with decrease in temperature (at a fixed μ) and increase in μ (at a constant temperature) because η is largely determined by the value of the RDF at contact, $g(\sigma)$.[36,37] The small increase of RDF peak value, however, suggests that enhancement of liquid structure upon switching on of the solvent–solvent dipolar interaction. Diffusion coefficient is then expected to reflect this enhanced solvent structure of SM fluids. The similarity in the RDFs obtained earlier by using the hard sphere and L–J potentials have already indicated the dominance of liquid structure by the repulsive part of the potential.[38] In addition, the well-depth of the L–J potential have secondary effects on the height of the first peak of the calculated $g(r)$.[39] A small increase in the simulated $g(r)$ with μ in the present study is therefore in accordance with earlier results obtained for model fluids.

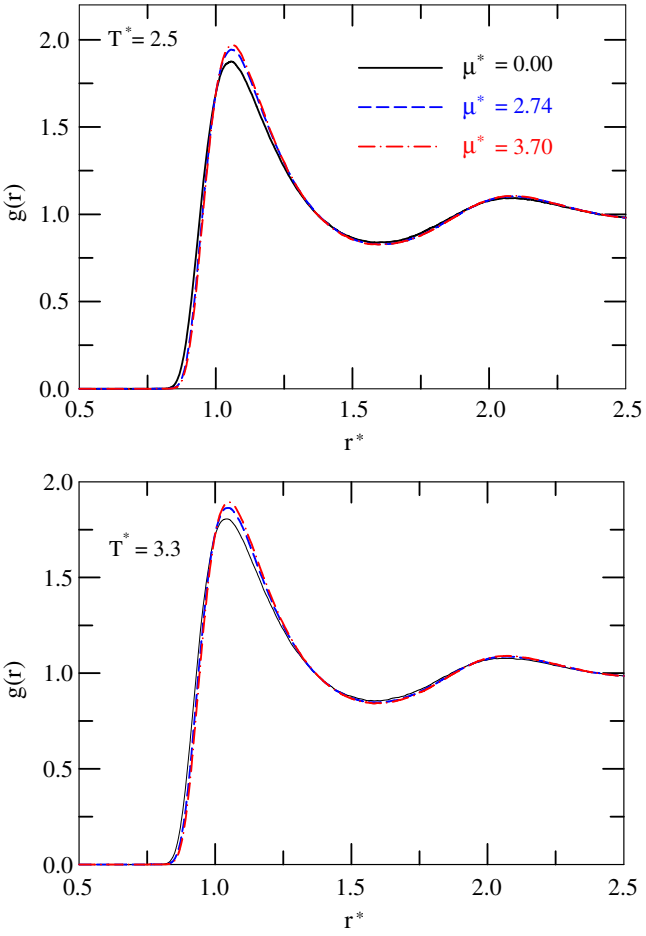

Figure 1. Plots of simulated radial distribution function for systems with different dipole moments. Two panels are for two different temperatures. Different curves are colour-coded and explained in the respective panels.

Average mean square displacements (MSDs) obtained for L–J and two SM fluids at two different temperatures are presented in figure 2, where the simulated $\left\langle |\Delta\vec{r}\,(t)|^2 \right\rangle$ are shown as a function of the scaled time, $t^* = t/\sqrt{m\sigma^2/\varepsilon}$. Clearly, the slope of the $\left\langle |\Delta\vec{r}(t)|^2 \right\rangle$ versus t^* decreases with increase in μ, indicating decrease in translational diffusion coefficient (D_T) as the L–J fluid is replaced by the SM ones. However, the plots in the lower panel suggest that effects of dipole moment become weaker as increase in temperature induces loosening of the liquid structure. The enhancement of decay rates of the normalized velocity autocorrelation function with μ, shown in figure 3, further reflects the effects of solution structure and 'loosening' of it upon temperature-rise on particle diffusion. Physically this can be understood by realizing that the enhanced solvent structure upon switching on of the dipolar interaction decorrelates the velocity vector at any given time from that at the beginning rather quickly through increased collision against the environment. Eventhough no analytical theory or simulations exist for neat dipolar systems that have investigated the dependence of collision frequency with μ, theoretical studies with (ion + dipole) binary mixtures have predicted linear dependence of collision frequency with the dipole moment of the polar species at a fixed temperature.[40,41]

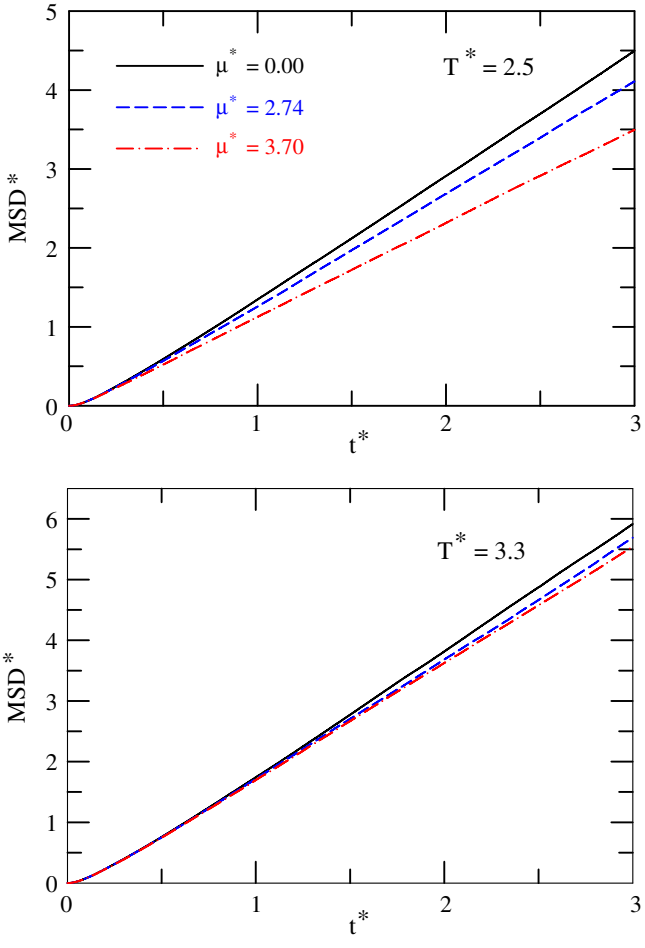

Figure 2. Simulated mean square displacements (MSDs) as a function of time at two different temperatures. Note the dipole moment dependence, particularly at the lower temperature.

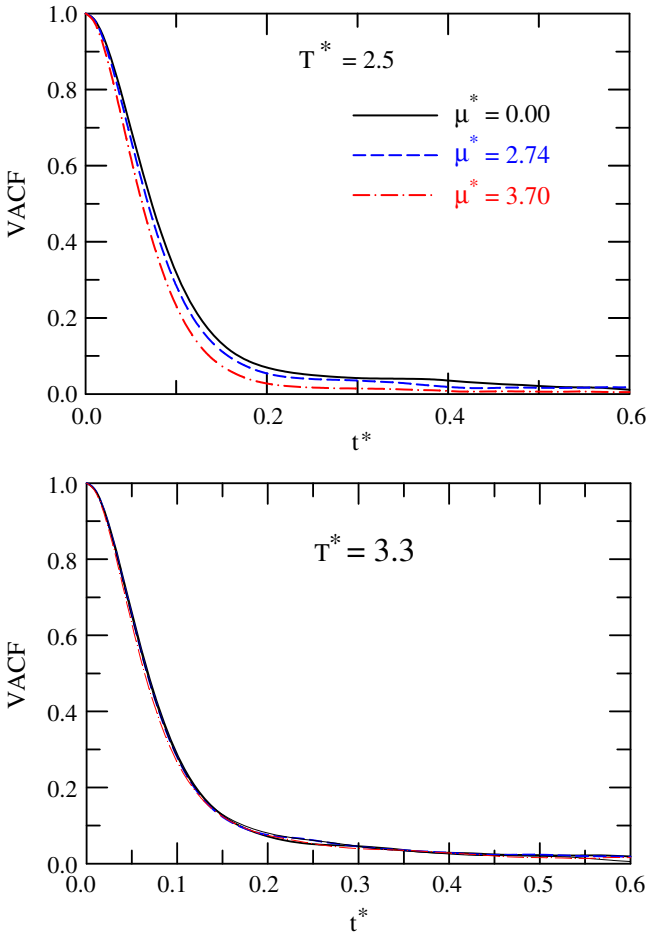

Figure 3. Simulated velocity autocorrelation functions (VACFs) as a function of time for systems with different dipole moments at two different temperatures.

Figure 4 presents the simulated translational diffusion coefficient of a tagged solvent particle $\left(D_T^* = D_T\sqrt{m/\sigma^2\varepsilon}\right)$ as a function of dipole moment $\left(\mu^* = \sqrt{\mu^2/\sigma^3\varepsilon}\right)$ for three different temperatures ($T^* = k_BT/\varepsilon$). D_T^* shown here are the arithmetic means of the values obtained via the MSD and VACF routes. As expected, particle diffusion is larger at higher temperature when all other thermodynamic parameters kept fixed. However, note that the dependence on dipole moment of D_T^* becomes weaker at

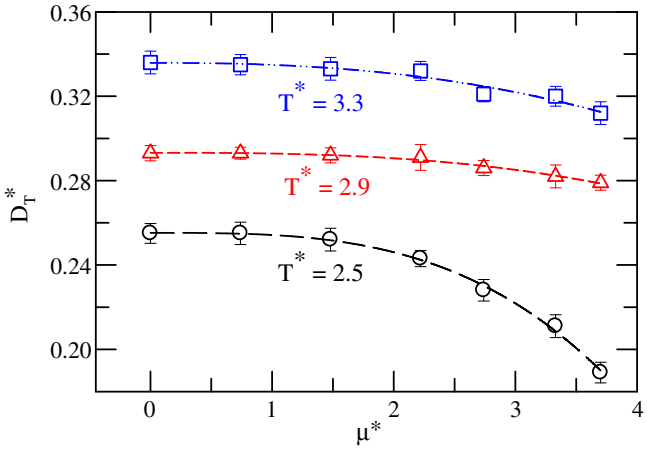

Figure 4. Dipole moment dependence of simulated translational diffusion coefficient at three different temperatures. Error bars have been computed via block average and they represent standard deviations about the respective mean values. Lines going through the data are for visual guide. Note that the extent of variation with μ^* at a given T^* is small and becoming even smaller at higher temperature.

indicates that the liquid structure is indeed governed by the shorter-ranged interactions where the longer-ranged dipolar interactions have minimal effects on the liquid structure that dictates diffusion.

Figure 5 shows the effects of dipole moment on rotational diffusion at three different temperatures. The interesting aspect to note here is that $D_R^*\left(=D_R\sqrt{m\sigma^2/\varepsilon}\right)$ is much more insensitive to μ^* than what has been observed for D_T^* as shown in figure 4. The microscopic reason for such a behaviour arises from the dipole moment insensitivity of the decay of angular velocity autocorrelation function (AVCF), shown in figure 6. The AVCF decays presented in two panels of figure 6 for two different temperatures demonstrate insignificant effects of dipole moment. In contrast, VACF decays and MSDs, particularly those at lower temperatures, exhibit much stronger μ^* dependence. The difference lies in the fact that while breaking of solvent structure is necessary for translational

higher temperature. This can be understood from the temperature dependencies of the simulated MSD and VACF already shown in figures 2 and 3, and originates from the less rigid solvent structure at higher temperature. If parameters for argon is used to calculate diffusion coefficient from the simulated data for L–J systems (that is at $\mu^* = 0$) at $T^* = 2.5$, we find $D_T \approx 1.4 \times 10^{-4}\,\mathrm{cm^2\,s^{-1}}$, a value in semi-quantitative agreement to earlier simulation results obtained by using 108 L–J particles at comparable density and temperature.[42] The insensitivity to dipole moment of D_T^* in the $0 \le \mu^* \le 1.5$ range at these temperatures, however,

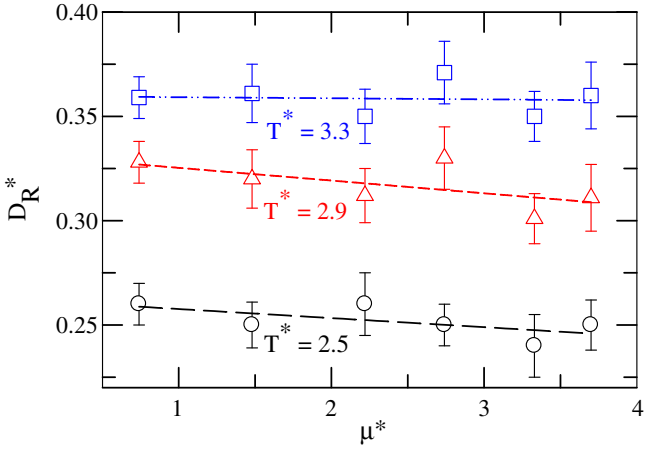

Figure 5. Dipole moment dependence of rotational diffusion coefficient at three different temperatures. As in figure 4, error bars have been determined via block averaging.

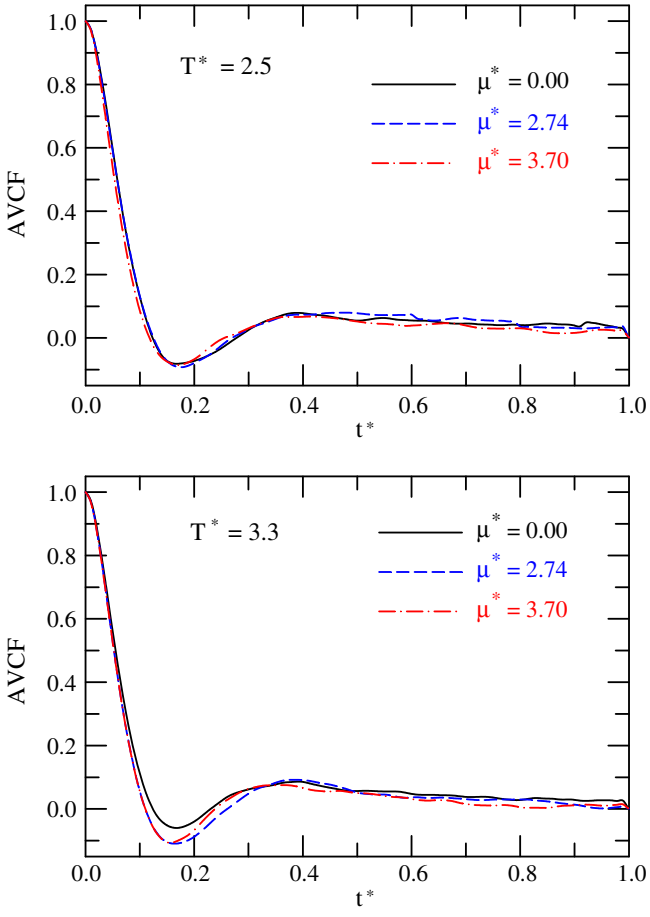

Figure 6. Plots of angular velocity correlation functions (AVCFs) as a function of time at two different temperatures. For further details, see the text.

diffusion, rotational diffusion does not require centre-of-mass motion and thus can remain largely immune to whatever effects that the longer-ranged dipolar interactions might have on solvent structure. Given that the only friction on rotational motion arises from the dipolar interactions, the modest changes for D_R^* from the lowest μ^* indicate that the molecules are nearly free rotors in all cases. This feature makes the rotations in the model somewhat different from that of most molecular liquids.

As presented in the upper panel of figure 7, the simulated viscosity as a function of dipole moment at $T^* = 2.5$. It is clear from this figure that η^* rises rather rapidly with μ^* particularly at the high end and the increase could be as large as ~60% over the value of the corresponding L–J fluid. This suggests that the longer-ranged dipole–dipole interaction does affect the medium viscosity, and the effects become stronger for systems with higher dipole moments. As the lower panel of this figure suggests, the increase of η^* with μ^* at a fixed temperature and density emerges from the steady increase of the value at $t^* = 0$ of the pressure autocorrelation function (PACF) with dipole moment. We would like to mention here that, η^* being more collective in nature than diffusion coefficient (D_x^*), simulations of the former is trickier than the latter and the simulated η^* values are often associated with larger error bars, particularly those covering the temperature range considered here.[42] As a result, the present simulations have not been able to capture quite cleanly the temperature dependence of viscosity coefficient as observed for real liquids. However, the dependence of the simulated η^* on μ^* at the other two higher temperatures ($T^* = 2.9$ and 3.3) remained qualitatively the same as that observed at $T^* = 2.5$. When compared for L–J argon (that is, at $\mu^* = 0$) at 300 K, the present simulations predict $\eta \approx 1.1 \times 10^{-3} P$ which is in satisfactory agreement with earlier simulation results.[42] This and the agreement found for translational diffusion coefficient earlier provides us with the necessary confidence that the present simulations have been carried out properly.

Figure 8 shows the simulated mean pressure $\left(P^* = P\sigma^3/\varepsilon\right)$ as a function of μ^* for the three temperatures considered. The dependence of P^* on μ^* can be understood from Eq. 9 which predicts, in the limit of low μ^*, a linear dependence on T^*. At higher μ^*, however, quadratic dependence on dipole moment supersedes the linear temperature dependence and P^* changes approximately as μ^{*2}. This is also the reason

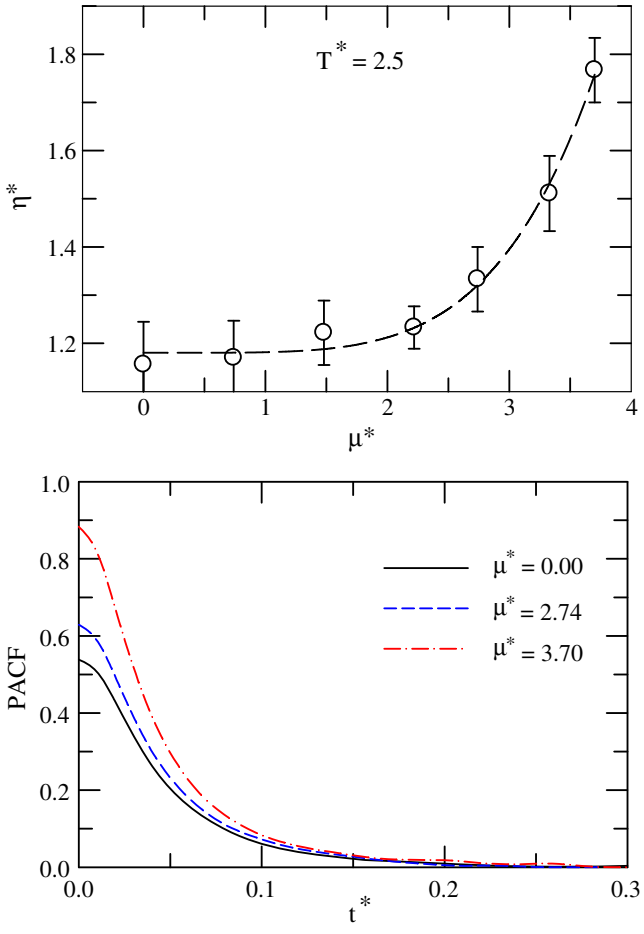

Figure 7. Effects of dipole moment on simulated viscosity (upper panel) and on pressure autocorrelation function, PACF (lower panel). Time integration of this correlation function (multiplied by a prefactor) provides the numerical values for the shear viscosity coefficient.

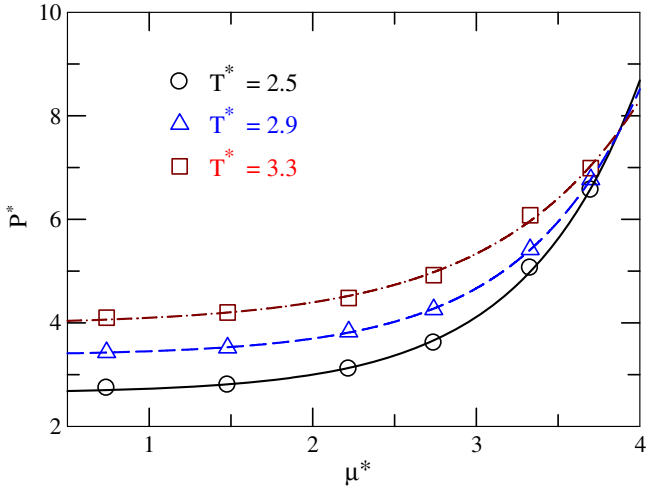

Figure 8. Dipole moment dependence of simulated mean pressure for SM fluids at three different temperatures. While the symbols represent simulated values, lines going through them act as visual guides. Circles, triangles and squares represent data at $T^* = 2.5$, 2.9 and 3.3, respectively.

for η^* showing nearly a μ^{*2} dependence at large dipole moments (upper panel, figure 7) at a given temperature.

Next we investigate in figure 9 the applicability of the SE and the SED relations where we show the simulated dipole moment dependence of the diffusion coefficient multiplied by the temperature-scaled viscosity coefficient $\left(D_x^* \times \eta^*/T^*\right)$. This scaled quantity, $D_x^* \times \eta^*/T^*$, is expected to be constant with μ^* for a given particle if the above hydrodynamic relations (SE and SED) remain valid. Earlier simulations have already suggested that such hydrodynamic relations hold in a broad range of density and temperature for pure simple fluids where solute-to-solvent size and interaction ratios are unity.[43] The nature of the curves in the panels of figure 9 (shown without error bars for the sake of clarity) strongly suggest break-down of SE and SED relations for Stockmayer fluids. The rise of $D_x^* \times \eta^*/T^*$ with μ^* arises because the increase in η^* is not equally reciprocated by the decrease in D_x^*, signalling a partially decoupling between these two transport coefficients. Several

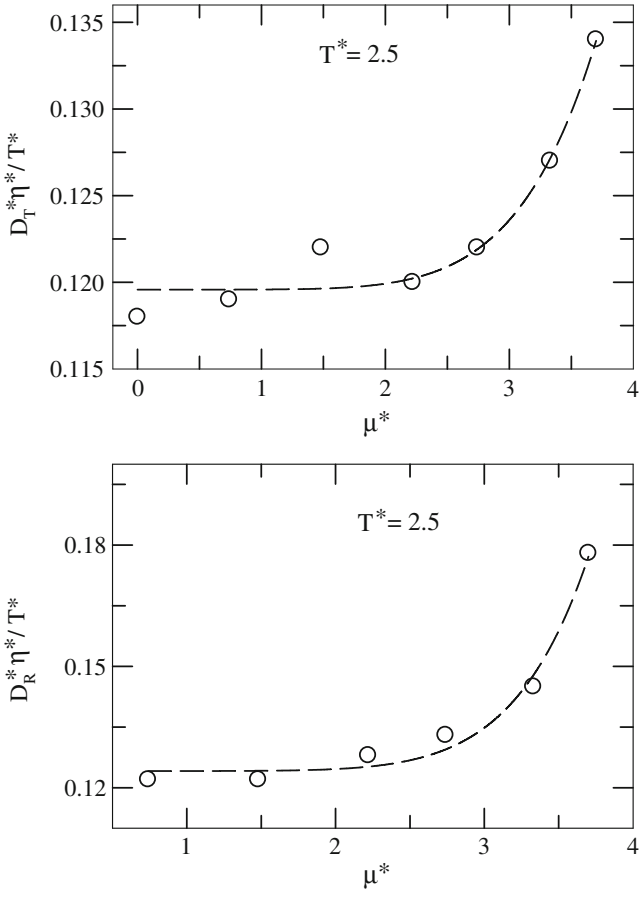

Figure 9. Deviation from the Stokes–Einstein and Stokes–Einstein–Debye relations for the simulated translational (upper panel) and rotational diffusion coefficients (lower panel) as a function of dipole moment.

works in the last few years have shown that breaking down of the hydrodynamic relations may occur for diverse systems ranging from as simple as hard sphere or L–J fluids[44–48] to as complex as sucrose benzoate,[49] supercritical fluids[50] and ionic liquids.[51–53] The deviations from the SE and SED relations therefore suggest that diffusion-viscosity decoupling is not an exclusive aspect of deeply supercooled systems where dynamic heterogeneity is traditionally attributed to the observed decoupling,[54,55] different rate of particle motions may play an important role as well in deciding environmental coupling in these model systems at temperatures much away from supercooling.

The presence of dynamic heterogeneity is next investigated for these model systems by following the deviation of the self-part of the van Hove correlation function, $G_s(\vec{r}, t)$, at intermediate times (times between inertial and diffusive regimes) from the Gaussian distribution with respect to particle displacement, and a non-Gaussian parameter, $\alpha(t)$.[56–58] The time-dependent self-part of the van Hove correlation function is give as[1,9]

$$G_s(\vec{r}, t) = \frac{1}{N}\left\langle \sum_{i=1}^{N} \delta\left(\vec{r}_i^{\,c}(t) - \vec{r}_i^{\,c}(0) - \vec{r}\right)\right\rangle, \qquad (10)$$

where r^c denotes the centre-of-mass of a particle. The Maxwell–Boltzmann velocity distribution at extermely short time (that is, $t \to 0$) and hydrodynamic behaviour at $t \to \infty$, forces $G_s(\vec{r}, t)$ to be Gaussian with particle displacement, $\Delta\vec{r}(t)$. The non-Gaussian parameter is defined as follows[58]

$$\alpha(t) = \frac{3}{5}\frac{\left\langle |\Delta\vec{r}(t)|^4\right\rangle}{\left\langle |\Delta\vec{r}(t)|^2\right\rangle^2} - 1, \qquad (11)$$

with $\left\langle |\Delta\vec{r}(t)|^2\right\rangle = \frac{1}{N}\left\langle \sum_{i=1}^{N} \left|\vec{r}_i^{\,c}(t) - \vec{r}_i^{\,c}(0)\right|^2\right\rangle$. For homogeneous harmonic vibrations and in the cases of random walk, $G_s(\vec{r}, t)$ is Gaussian and $\alpha(t) = 0$.[9] For hot liquids, $\alpha(t) = 0$ for both at $t = 0$ and $t = \infty$ but $\alpha(t) = 0.2$ (a maximum) at intemediate times.[9]

The simulated $\alpha(t)$ and $G_s(\vec{r}, t)$ are presented in figure 10 for SM fluids with $\mu^* = 0.74$ and 3.70. At $T^* = 2.5$ for SM fluid with $\mu^* = 3.7$, simulated $\alpha(t)$ curve shows a rather sharp peak at $t^* \approx 200$ which indicates the presence of a substantial degree of dynamic heterogeneity in this fluid. Interestingly, the peak vanishes at $T^* = 3.3$, indicating 'homogenization' of particle motions upon raising the solution temperature. In addition, for SM fluids with $\mu^* = 0.74$ at $T^* = 2.5$, $\alpha(t)$ remains structureless for the entire simulation period. The displacement statistics

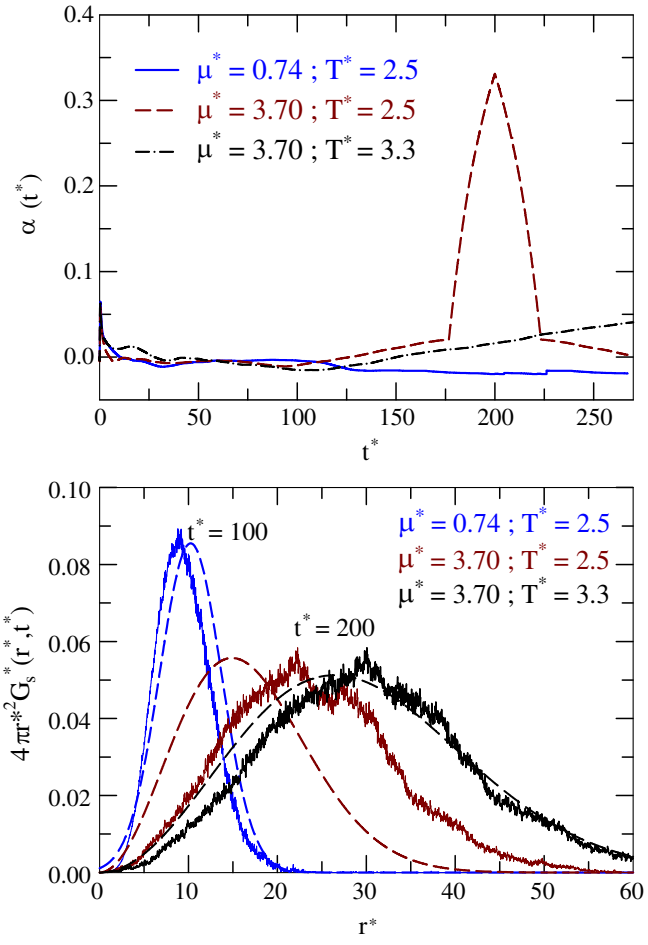

Figure 10. Signatures of dynamic heterogeneity in SM fluids and its temperature and dipole moment dependencies. Upper panel shows plots of the simulated non-Gaussian parameter, $\alpha(t)$, associated with centre-of-mass motion of particles for three different values of dipole moment. Curves are colour-coded. Note the simulated $\alpha(t^*)$ at $\mu^* = 0.74$ appears to go slightly below zero which may occur due to limited averaging. This may also be the reason for the 'not-so-smooth' character of the $\alpha(t^*)$ peak obtained at $\mu^* = 3.70$ and $T^* = 2.5$. Lower panel depicts the deviation from Gaussian statistics for particle displacements for SM fluids with different dipole moments and temperatures. As before, the curves are colour-coded. While the simulated curves are shown by solid lines, dashed lines denote calculations using the following Gaussian approximation[9,35]: $G_s^0(r,t) = \left[3/2\pi \left\langle|\Delta\vec{r}(t)|^2\right\rangle\right]^{3/2} \exp\left(-3r^2/\left(2\left\langle|\Delta\vec{r}\,(t)|^2\right\rangle\right)\right)$.

shown in the lower panel clearly reveals a significant deviation for the simulated $G_s(\vec{r},t)$ at $t^* \approx 200$ from the predicted Gaussian behaviour for SM fluid at $T^* = 2.5$ with $\mu^* = 3.7$ but becomes closer to the Gaussian approximation (dashed lines) either upon decreasing the dipole moment or increasing the solution temperature. The variation of dynamic heterogeneity with dipole moment and temperature for SM fluids therefore explains in microscopic terms (i) the weakening of dipole moment effects on translational diffusion coefficient upon temperature-rise (shown in figure 4) and (ii) deviation from the SE behaviour for SM fluids with larger dipole moment at relativley lower temperature.

4. Conclusion

In this paper, the dipole-moment dependence of transport properties have been studied by molecular dynamics simulations. Medium viscosity has been found to increase as large as by ∼60% with dipole moment over the value for the corresponding L–J system at a fixed density and temperature. While the translational diffusion coefficients show a moderate dipole moment dependence which softens up upon increasing the solution temperature, rotational diffusion coefficients appear to be insensitive to the magnitude of dipole moment. The different dependence of the translational and rotational diffusion coefficients has been found to originate from the different sensitivity of the mean square displacements and angular velocity autocorrelation functions to the dipolar interactions. Simulated diffusion coefficients have been found not to follow the conventional hydrodynamic relations with the simulated viscosity coefficients, supporting the notion that break-down of these relations is more widespread than expected. Simulated particle motions at intermediate time have been found to show a substantial deviation from the Gaussian distribution (with respect to particle displacements) for SM fluids with larger dipole moment which reverts back to approximately Gaussian behaviour upon either rising the temperature or lowering the dipole moment.

Since the present work has explored the relationship between transport coefficients which are collective properties, a discussion on system size dependence is very much relevant and important.[59] There are several in-depth studies[12,46,60,61] exploring system size dependences of diffusion coefficients and viscosity and subsequent determination of the stick-slip boundary conditions.[61] All these studies have found, depending upon density and interaction potentials, moderate to small system size dependences. At higher densities like the one considered here, effects of number of particles have been found generally small. Therefore, the numerical values for the transport coefficients reported in the present work may slightly vary if compared with simulations using larger number of particles. However, those variations will not affect the qualitative features reflected by the present simulation study.

Acknowledgements

We thank Prof. A K Raychaudhuri, S N Bose National Centre for Basic Sciences, for kindly bringing this problem to our attention. SD acknowledges the Council of Scientific and Industrial Research (CSIR), India for a research fellowship. We thank Prof. M Maroncelli and Dr. H K Kashyap for useful comments and discussion.

References

1. Hansen J P and McDonald I R 1986 *Theory of simple liquids* (London: Academic Press)
2. Lakowicz J R 1999 *Principles of fluorescence spectroscopy* (New York: Kluwar Academic /Plenum)
3. Ediger, M D 2000 *Annu. Rev. Phys. Chem.* **51** 99
4. Chakrabarti, D and Bagchi B 2006 *Phys. Rev. Lett.* **96** 187801
5. Abraham S E, Bhattacharyya S M and Bagchi B 2008 *Phys. Rev. Lett.* **100** 167801
6. Guchhait B, Gazi H A R, Kashyap H K and Biswas R 2010 *J. Phys. Chem. B* **114** 5066
7. Gazi H A R, Guchhait B, Daschakraborty S, Biswas R 2011 *Chem. Phys. Lett.* **501** 358
8. Guchhait B, Daschakraborty S, Biswas R 2012 *J. Chem. Phys.* **136** 174503
9. Pal T and Biswas R 2011 *Chem. Phys. Lett.* **517** 180
10. Kirkpatrick T R 1984 *Phys. Rev. Lett.* **53** 1735
11. Kirkpatrick T R 1985 *J. Non-Cryst. Solids* **75** 437
12. Meier K, Laesecke A, Kabelac S 2005 *J. Chem. Phys.* **122** 014513
13. Mukherjee A, Bhattacharyya S, Bagchi B 2002 *J. Chem. Phys.* **116** 4577
14. Bendrov D, Smith G D, Sewell T D 2000 *J. Chem. Phys.* **112** 7203
15. Biswanath D S 2007 *Viscosity of liquids: Theory, estimation, experiment and data* (The Netherland: Springer)
16. Stockmayer W H 1941 *J. Chem. Phys.* **9** 398
17. Vesely F J 1977 *J. Comput. Phys.* **24** 361
18. Khordad R, Hosseini F and Papari M M 2009 *Chem. Phys.* **360** 123
19. Pollock E L and Alder B J 1980 *Physica* **102A** 1
20. Pollock E L, Alder B J and Patey G N 1981 *Physica* **108A** 14
21. Gray C G, Sainger Y S, Joslin C G, Cummings P T and Goldman S 1986 *J. Chem. Phys.* **85** 1502
22. Neria E and Nitzan A 1992 *J. Chem. Phys.* **96** 5433
23. Perera L and Berkowitz M L 1992 *J. Chem. Phys.* **97** 5253
24. Roy S and Bagchi B 1993 *J. Chem. Phys.* **99** 1310
25. Chandra A 1995 *Chem. Phys. Lett.* **235** 133
26. Stevens M J and Grest G S 1995 *Phys. Rev. E* **51** 5962
27. Gao G T and Zeng X C 2000 *Phys. Rev. E* **61** R2188
28. Paul S and Chandra A 2003 *J. Phys. Chem. B* **107** 12705
29. Paul S and Chandra A 2007 *J. Phys. Chem. B* **111** 12500
30. Allen M P and Tildesley D J 1987 *Computer simulations of liquids* (New York: Oxford University Press)
31. Nosé S 1984 *J. Chem. Phys.* **81** 511
32. Evans D J and Holian B L 1985 *J. Chem. Phys.* **83** 4069
33. Frenkel D and Smit B 1996 *Understanding molecular simulation: from algorithm to applications* (San Diego, USA: Academic Press)
34. McQuarrie D A 2003 *Statistical mechanics* (New Delhi: Viva Books)
35. Del Popolo M G and Voth G A 2004 *J. Phys. Chem. B* **108** 1744
36. Boon J P and Yip S 1980 *Molecular hydrodynamics* (New York: McGraw-Hill)
37. Biswas R and Bagchi B 1996 *J. Chem. Phys.* **105** 7543
38. Goharshadi E K and Mansoori A G 2007 *Chem. Phys.* **331** 332
39. Matteoli E and Mansoori G A 1995 *J. Chem. Phys.* **103** 11
40. Turulski J and Forys M 1979 *J. Phys. Chem.* **83** 22
41. Ridge D P and Beauchamp J L 1976 *Chem. Phys. Lett.* **41** 2
42. Borgelt P, Hoheisel C and Stell G 1990 *Phys. Rev. A* **42** 789
43. Cappelezzo M, Capellari C A, Pezzin S H and Coelho L A F 2007 *J. Chem. Phys.* **126** 224516
44. Harris K R 2009 *J. Chem. Phys.* **131** 054503
45. Meier K, Laesecke A and Kabelac S 2004 *J. Chem. Phys.* **121** 3671
46. Meier K, Laesecke A and Kabelac S 2004 *J. Chem. Phys.* **121** 9526
47. Sharma M and Yashonath S 2006 *J. Phys. Chem. B* **110** 17207
48. Kumar S K, Szamel G and Douglas J F 2006 *J. Chem. Phys.* **124** 214501
49. Rajian J R, Huang W, Richert R and Quitevis E L 2006 *J. Chem. Phys.* **124** 014510
50. Funazukuri T, Kong C Y and Kagei S 2008 *J. Supercrit. Fluids* **46** 280
51. Kanakubo M, Harris K R, Tsuchihashi N, Ibuki K, Ueno M 2007 *J. Phys. Chem. B* **111** 2062
52. Kanakubo M, Harris K R, Tsuchihashi N, Ibuki K, Ueno M 2007 *J. Phys. Chem. B* **111** 13867
53. Harris K R, Kanakubo M, Tsuchihashi N, Ibuki K, Ueno M 2008 *J. Phys. Chem. B* **112** 9830
54. Sillescu H 1999 *J. Non-Cryst. Solids* **243** 81
55. Kumar P, Buldyrev S V, Becker S R, Poole P H, Starr F W and Stanley H E 2007 *Proc. Natl. Acad. Sci. USA* **104** 9575
56. Wang Y, Voth G A 2005 *J. Am. Chem. Soc.* **127** 12192
57. Roy D, Patel N, Conte S and Maroncelli M 2010 *J. Phys. Chem. B* **114** 12629
58. Rahman A 1964 *Phys. Rev.* **136** 405
59. Sigurgeirsson H and Heyes D M 2003 *Mol. Phys.* **101** 469
60. Yeh I-C and Hummer G 2004 *J. Phys. Chem. B* **108** 15873
61. Heyes D M 2007 *J. Phys.: Condens. Matter* **19** 376106